Materials and Design 195 (2020) 109049

Contents lists available at ScienceDirect

Materials and Design

journal homepage: www.elsevier.com/locate/matdes

Rubbery nanofibrous interleaves enhance fracture toughness and damping of CFRP laminates

Emanuele Maccaferri [a], Laura Mazzocchetti [a,b,*], Tiziana Benelli [a,b], Tommaso Maria Brugo [b,c], Andrea Zucchelli [b,c], Loris Giorgini [a,b,*]

[a] Department of Industrial Chemistry "Toso Montanari", University of Bologna, Viale Risorgimento 4, 40136 Bologna, Italy.
[b] Interdepartmental Center for Industrial Research on Advanced Applications in Mechanical Engineering and Materials Technology, CIRI-MAM, University of Bologna, Viale Risorgimento 2, 40136 Bologna, Italy.
[c] Department of Industrial Engineering, University of Bologna, Viale Risorgimento 2, 40136 Bologna, Italy.

HIGHLIGHTS

- NBR/PCL blend nanofibrous mats hinder delamination of epoxy-based CFRP laminates via localized resin toughening.
- Dramatic increase of the energy release rate (G) at the initiation and propagation stages (up to 5.8× and 4.4× the reference values, respectively) is observed.
- The rubbery mats are able to blend with the epoxy matrix during curing, providing a significant modification of the damping ability.
- Depending on the specific application, the percentage of rubber should be carefully tuned in order to obtain the best compromise between damping and maximum operating temperature.
- Rubbery nanofibrous mats can be applied for localized modification of laminates in critical spots, such as free edges, holes, ply-drops and adhesive bonding.

GRAPHICAL ABSTRACT

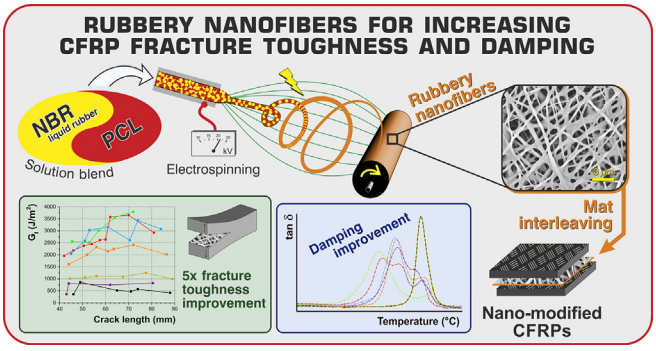

ARTICLE INFO

Article history:
Received 9 June 2020
Received in revised form 5 August 2020
Accepted 6 August 2020
Available online 12 August 2020

Keywords:
CFRP
Nanofibers
Rubber
Delamination
Damping
Electrospinning

ABSTRACT

Rubbery electrospun nanofibers represent a smart way for hindering delamination and enhancing damping capacity in Carbon Fiber Reinforced Polymer (CFRP) laminates, which are two of the most serious drawbacks hampering their use. Nitrile Butadiene Rubber / Poly(ε-caprolactone) (NBR/PCL) blend nanofibers, with 20-40-60%wt of not crosslinked NBR, were interleaved in epoxy-based CFRPs to evaluate their effect on the final composite performance. CFRPs with rubbery mats show a significant increase of the energy release rate in Mode I, both at initiation and propagation stages (+480% and +340%, respectively), thanks to NBR/PCL blend ability to promote high matrix toughening of the fragile epoxy resin. In Mode II a maximum improvement of about 30% was achieved. The presence of highly damping NBR component widens the composite energy dissipation window below room temperature, enhancing the CFRP damping. Similar results were obtained with two different epoxy resins, and the effect of the layering sequence was also discussed. NBR percentage in nanofibers and nanofibrous mats amount may strongly affect the CFRP maximum operating temperature. Nanofibers can be

* Corresponding authors.
E-mail addresses: laura.mazzocchetti@unibo.it (L. Mazzocchetti), loris.giorgini@unibo.it (L. Giorgini).

https://doi.org/10.1016/j.matdes.2020.109049

positioned, during lamination, in the critical regions where interlaminar stresses are mostly concentrated due to geometric discontinuities providing a flexible approach to localized modification of laminates.

1. Introduction

Even though Carbon Fiber Reinforced Polymers (CFRPs) display a number of attractive mechanical properties, being often thermoset based, they are very stiff materials, whose main failure modes are due to delamination at the interlaminar matrix-rich region [1,2]. Such a high stiffness implies also low damping capacity which, in turn, results in structure-borne noise and undesirable vibrations that may contribute to delamination triggering [3], limiting their use for example in automotive applications [4]. Among the most critical materials in terms of brittleness, the highly cross-linked epoxy resins are quite renown [5], and rubber toughening has been since decades one of the favourite approaches to solve, or limit, this issue [6]. Toughening is often attained by addition of about 5–20%wt rubbery particles either crosslinked, for which a core-shell morphology with rubbery core and glassy shell is required, or via mixing polymeric precursors with liquid rubber (i.e. not crosslinked) with precipitation of the latter during resin cross-linking thus forming rubbery particles on site [5–9]. However, in both cases, the rubber fraction required to attain a suitable toughening might detrimentally impact other substantial structural properties such as the high glass transition temperature (T_g), high tensile strength, high modulus and premium dimensional stability typical of the epoxy systems [5]. An efficient alternative way to modify epoxy resin, proposed in 2001 [10], makes use of nanofibrous membranes [11–14], acting both as resin toughening agents, as well as bridging threads that help keeping the diverging edges together, reaching significant increase in the delamination energy release rate at initiation ($G_{I,C}$ or $G_{II,C}$) and propagation ($G_{I,R}$ or $G_{II,R}$) stages [13,15]. Beside toughening, nanofibers can also impart a lot of different functional properties [16], and they appear as a smart approach to locally modify the resin only where required, without affecting the overall bulk material and without the need to chemically modify the whole resin formulation [17]. Indeed, interlaminar stresses in a structural component develop in specific and localized areas, due to geometric discontinuities, such as free edges, holes, ply-drops and adhesive bonding [18]. Rubber toughening, especially if promoted by submicron sized materials [19], may also enhance the composite behaviour at low temperature [20], where the negative effect of stress is amplified by the natural increase of matrix brittleness, which tends to favor microcracking [21,22].

Another important CFRP feature that can be improved by rubbery materials is their damping, frequently pursued by addition of bulk (cross-linked or thermoplastic) rubbery films, applied to attain reasonable vibrations hampering, often at the cost of the overall stiffness and integrity [21]. In this frame the use of rubbery nanofibers might increase both toughness, and damping, without excessively affecting the overall mechanical performance of the material or significantly increase its weight and size. Yet, to the best of the Authors' knowledge, no literature exists about the use of rubbery fibers for CFRP modification. While rubbery materials (such as Nitrile Butadiene Rubber, NBR) are well renowned for their damping [23] thanks to the high tanδ values, they cannot be easily formed in nanofibers, due to the low glass transition temperature (T_g) of the spinnable uncross-linked precursors which promote filming of the fibers within minutes from the spinning [24]. However, the Authors recently reported the possibility of obtaining "liquid" (i.e. not crosslinked) rubbery nanofibers (carboxylated-NBR, a polymer with good affinity for epoxy resin precursors) upon blending with a convenient polymeric coadjutant such as poly(ε-caprolactone) (PCL) [24]. In this work, thus, the use of electrospun "liquid" rubber NBR/PCL blends nanofibrous mats is reported as an innovative material for producing toughened CFRPs laminates. Hence NBR/PCL nanofibers with different blend compositions were interleaved among prepregs during CFRP panels production with tailored stacking sequences in order to evaluate the "liquid" rubber effect on the final CFRP mechanical performance. For the sake of comparison, laminates modified with plain PCL nanofibers and NBR film were produced. Moreover, a CFRP panel with interleaved Nylon 66 nanofibers, largely used for hindering delamination [15], was also obtained in order to compare its performance with rubbery nanofibers modified composites. Two different epoxy matrices were used to evaluate the effect of rubbery nanofibers on different thermosets. The interlaminar fracture toughness of laminates was assessed by Mode I and II loadings tests (evaluation of the energy release rate G_I and G_{II}, respectively). The damping behaviour of laminates was investigated via dynamic mechanical analysis (DMA). The use of interleaved nonwoven layers in composite laminates is proposed since years. Nonetheless, usually the investigation is limited to the evaluation of delamination performances or damping at room temperature [15,25]. The thermomechanical behaviour assessment over a wide range of temperatures is fundamental for determining the possible fields of application of the material, highlighting strengths and weaknesses. To this end, DMA was performed to understand the impact of such nanomodification not only on the damping, but also on the overall thermomechanical properties of the laminate, depending also on the number of modified interfaces and the properties of the hosting epoxy resin. In Fig. 1 is depicted a sketch of the paper rationale.

2. Materials and methods

2.1. Materials

Carboxylated nitrile butadiene rubber (NBR) NIPOL 1072CGX was purchased from Zeon Chemicals [68%mol butadiene (Bu), 28%mol acrylonitrile (ACN), 4%mol methacrylic acid (MAA)]. Poly(ε-caprolactone) (PCL), M_w 70,000-90,000, was purchased from Sigma-Aldrich. Nylon 66 Zytel E53 NC010, kindly provided by DuPont, was dried in a stove at 110 °C for minimum 6 h before use. *N,N*-dimethylacetamide (DMAc), *N,N*-dimethylformamide (DMF), formic acid and chloroform ($CHCl_3$) were purchased from Sigma-Aldrich and were used without any preliminary treatment. Plain weave carbon fabric (200 g/m^2) in epoxy matrices with two different glass transition temperatures (GG204P IMP503Z and "High Temperature" GG204P IMP503Z-HT) prepregs for composite lamination were supplied by G. Angeloni s.r.l. (Venezia, Italy).

2.2. Nanofibers and CFRP panels production

Nanofibrous mats were produced via single-needle electrospinning, according to a previously reported method from the Authors [24]; the composition and processing conditions are described in Supplementary Information (SI-S1). Nanofibers of NBR/PCL blends with different composition (labelled as *n*-X/Y, where *n* stands for "nanofibrous mat", X is the NBR weight fraction in the nanofiber and Y the PCL counterpart), as well as of plain Nylon 66 (labelled as *n*-NYL) and PCL (labelled as *n*-PCL) were obtained. A plain NBR compact film derived from the coalesced nanofibers (*f*-NBR, where *f* stands for "film") was produced. In Table 1 the produced membranes are reported, as well as the nanofibers diameter and the grammage of the mats, while the average membrane thickness is reported in Supplementary Information (Table SI-3).

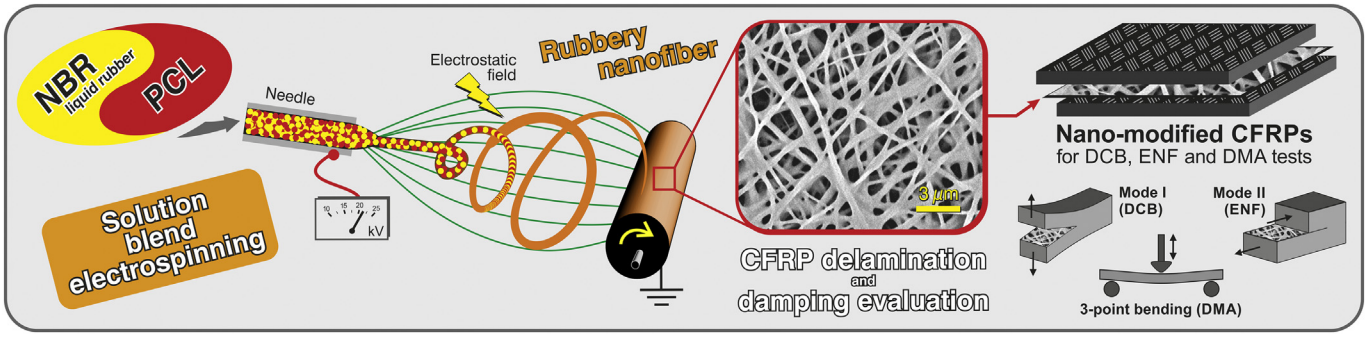

Fig. 1. – Sketch of the paper rationale: NBR/PCL blend nanofibers production by single-needle electrospinning process, mats integration in laminated CFRPs, and their testing for delamination, damping and thermomechanical properties evaluation.

Specimens for the interlaminar fracture toughness evaluation (DCB and ENF tests) were prepared via hand lay-up, stacking 14 prepreg plies (GG204P IMP503Z), interleaving a single nanofibrous mat in the central interface, and adding a Teflon film (Fig. SI-3) to allow the trigger for specimen delamination. Corresponding reference panels without nanofibrous membrane were also produced for the sake of comparison.

Composite panels are labelled as C-Z, where C stands for "composite" and Z represents just the composition of the abovementioned interleaved nanofibrous mat (*n*-X/Y, *n*-PCL, *n*-NYL). When NBR film (*f*-NBR) is used, the label of the composite keeps such indication (C-*f*-NBR) for better clarity. The unmodified composite, used as reference material, is labelled C-Ref. Uncured panels underwent a preliminary treatment of 2 h at 45 °C under vacuum for better nanofibers impregnation prior curing cycle in autoclave (2 h at 135 °C, under vacuum, 6 bar external pressure, heating/cooling ramp 2 °C/min).

CFRP panels for DMA tests (Fig. SI-1) were produced stacking 10 plies of GG204P IMP503Z prepregs. When the case, the membranes listed in Table 1 were placed within each ply, for a total of 9 integrated membranes, and also only in the central one. An unmodified reference panel for the sake of comparison (C-Ref) was produced too. Samples with a different number and a different positioning of *n*-60/40 mat were also produced with prepreg GG204P IMP503Z-HT (C-60/40-HT_*m*, where "*m*" accounts for the different number of the interleaved interfaces, as reported in detail in Table 2), together with an unmodified panel (C-Ref-HT). Details of the laminates production and dimensions are presented in SI-S2, while a list of the CFRPs produced is reported in Table 1.

2.3. Characterization of CFRPs

DCB and ENF tests were carried out using an Instron 5966 universal testing machine equipped with a 10 kN load cell, at room temperature (20 °C). DCB specimens were tested at 3.0 mm/min crosshead separation rate, while ENF at a displacement rate of 1.0 mm/min. At least 3 specimens for each CFRP material/delamination mode were tested. Detailed information about preparation, dimensions and testing of DCB and ENF specimens are reported in Supplementary Information (SI-S2).

DCB tests were performed in order to evaluate the energy release rate for Mode I loading (G_I, in J/m^2), both at the initial and propagation stages ($G_{I,C}$ and $G_{I,R}$, respectively), using the following formula [26]:

$$G_I = \frac{3P\delta}{2ba}1000$$

where P is the load (in N), δ the crosshead displacement (in mm), a the crack length (in mm), b the specimen width (in mm).

ENF tests were carried out for evaluating the fracture toughness in Mode II loading (G_{II}, in J/m^2), both at the initial and propagation stages ($G_{II,C}$ and $G_{II,R}$, respectively), using the following formula [27]:

$$G_{II} = \frac{9P\delta a^2}{2b\left(\frac{1}{4}L^3 + 3a^3\right)}1000$$

where P is the load (in N), δ the crosshead displacement (in mm), a the crack length (in mm), b the specimen width (in mm) and L the span length between supports (in mm).

Dynamic mechanical analysis (DMA) was carried out with a Netzsch DMA 242 E Artemis instrument in three-point bending deformation mode, using a 40 mm fixed span. DMA analysis in temperature ramp were carried out in the −85 +200 °C range at 3 °C/min heating rate, 1 Hz frequency, amplitude 20 μm, static force / dynamic force ratio = 1.5. DMA analyses in isothermal conditions were performed at 25, 35 and 45 °C, with temperature variations lower than 0.1 °C once stability was reached during tests. Instrument parameters were left all

Table 1
Laminated panels intended for DCB, ENF, DMA tests, and main membranes characteristics.

CFRP for DCB / ENF	CFRP for DMA		Interleaved membrane		Membrane grammage[a] (g/m^2)	Nanofiber diameter[b] (nm)
14 plies - IMP503Z resin 1 central mat + Teflon trigger	10 plies - IMP503Z resin 1 central mat / 9 mats	10 plies IMP503Z-HT resin	Membrane label	NBR fraction (%wt)		
C-Ref	C-Ref	C-Ref-HT	–	–	–	–
C-PCL	C-PCL	–	*n*-PCL	0	16.5 ± 1.5	402 ± 174
C-20/80	C-20/80	–	*n*-20/80	20	17.9 ± 1.2	247 ± 76
C-40/60	C-40/60	–	*n*-40/60	40	18.9 ± 1.2	216 ± 63
C-60/40	C-60/40	C-60/40-HT_*m* [c]	*n*-60/40	60	19.5 ± 1.5	259 ± 72
C-*f*-NBR	C-*f*-NBR	–	*f*-NBR	100	36.3 ± 1.6	–
C-NYL	C-NYL	–	*n*-NYL	–	11.2 ± 1.2	275 ± 69

[a] *Average values derived from at least 5 measurements in different membrane regions.*
[b] *Average values derived from at least 100 diameter measurements, manually done on single nanofibers by means of the Photoshop measurement tool.*
[c] *Various CFRP configurations: mats positioned in interface 5 (central), in 1–3–5-7-9 interfaces, and in all the interfaces (refer to Table 2 and Fig. 9B).*

Table 2
Laminated CFRP tested via DMA and their thermomechanical properties.

CFRP	Interleaved membrane	10 plies CFRP - 1 central mat IMP503Z resin			10 plies CFRP - 9 mats IMP503Z resin				10 plies CFRP IMP503Z-HT resin		
		E' below E' onset [a] (GPa)	E' onset (°C)	T_α [b] (°C)	E' below E' onset [a] (GPa)	E' at 25 °C (GPa)	E' onset (°C)	T_α [b] (°C)	E' below E' onset [a] (GPa)	E' onset (°C)	T_α [b] (°C)
C-Ref	–	34.5 ± 1.1	116 ± 1	129	34.7 ± 1.2	34.5 ± 1.1	116 ± 1	129	–	–	–
C-Ref-HT	–	–	–	–	–	–	–	–	41.2 ± 0.9	122 ± 2	150
C-PCL	*n*-PCL	32.9 ± 0.9	97 ± 2	125	33.4 ± 1.0	33.2 ± 1.1	51 ± 1	89	–	–	–
C-20/80	*n*-20/80	33.5 ± 1.2	92 ± 2	128	32.5 ± 1.2	32.2 ± 1.2	59 ± 2	87	–	–	–
C-40/60	*n*-40/60	33.1 ± 1.3	84 ± 1	127	32.8 ± 0.9	32.3 ± 1.2	49 ± 1	84	–	–	–
C-60/40	*n*-60/40	33.3 ± 1.3	82 ± 2	127	32.3 ± 1.1	31.0 ± 1.1	40 ± 2	63	–	–	–
C-60/40-HT_1 [c]	*n*-60/40	–	–	–	–	–	–	–	40.7 ± 1.2	103 ± 2	151
C-60/40-HT_5 [c]	*n*-60/40	–	–	–	–	–	–	–	38.2 ± 1.2	72 ± 2	151
C-60/40-HT_9 [c]	*n*-60/40	–	–	–	–	–	–	–	36.3 ± 1.1	61 ± 2	130
C-*f*-NBR	*f*-NBR	32.4 ± 1.2	53 ± 2	126	32.2 ± 1.0	25.7 ± 1.5	15 ± 1	58	–	–	–
C-NYL	*n*-NYL	33.4 ± 1.3	112 ± 1	129	34.0 ± 1.1	34.0 ± 1.1	117 ± 1	129	–	–	–

[a] *E' below E' onset was evaluated at 25 °C for CFRPs with only the central interface modified and for laminates with IMP503Z-HT, while for CFRPs with 9 mats interleaved at 0 °C (except for C-f-NBR at −25 °C).*
[b] *T_α corresponds to the main peak in tanδ curve, so it does not necessarily represent the tanδ peak positioned at the highest temperature. The standard deviation is not reported because it is lower than 1 °C for all the cases.*
[c] *Various CFRP configurations: mats positioned in interface 5 (C-60/40-HT_1), in 1-3-5-7-9 interfaces (C-60/40-HT_5), and in all the interfaces (C-60/40-HT_9).*

unchanged, but the testing frequencies, which in isothermal conditions are 1, 2.5, 5, 10, 20, 33.3 and 50 Hz. Tanδ values were obtained upon averaging 7 consecutive points recorded by the machine every 100 s (total time span about 12 min), after reaching temperature stability.

3. Results and discussion

With the aim of obtaining room temperature mechanically stable nanofibrous mats of thermoplastic rubbery materials, which would not require crosslinking after deposition, the NBR liquid rubber component (i.e. a rubber prior its crosslinking stage) was blended with PCL via single-needle electrospinning. A firm nanofiber morphology was obtained, and a NBR content of 60%wt in the electrospun material appears to be the threshold for good quality stable nanofibers (Fig. 2).

While NBR content up to 80%wt could be reached [24], the fibers were partially filmed and the handling of the membrane was difficult, hence NBR content higher than 60%wt was intentionally discarded. All nanofibers have sub-micrometric diameters, roughly ranging from 200 to 400 nm (Table 1), and good mechanical properties as previously assessed [24].

When nanofibers are included in CFRPs, they can affect dimension and weight of the composite differently from a bulk film. Indeed, fibrous mats are mainly made up of voids that can be impregnated by the resin precursors. In the present case, NBR/PCL blend fibers are expected to disappear upon curing since the fibers morphology is guaranteed solely by the presence of a PCL-like crystal phase that develops in the entire range of analyzed compositions and melts in the 55–65 °C range [24], i.e. well below the laminate curing temperature (135 °C).

Little to no influence is expected, and indeed is not observed, on CFRP weight and dimensions with just a single interleaved membrane. A different behaviour is shown by composites where all the interlaminae are modified with nanofibers (Table SI-3). When CFRP panel density is taken into account (Fig. SI-2A), addition of compact, crystalline and dense nanofibers, such as Nylon 66, and to a certain extent PCL too, is observed to impart a small reduction in the composite density, while addition of a rubbery free-volume rich component, such as NBR liquid rubber, leads to a more significant density decrease.

The higher the NBR fraction in nanofiber blends, the lower the attained CFRP density. Further density decrease is observed with plain *f*-NBR film, though in this case the membrane grammage is almost double with respect to rubbery nanofibrous membranes (Table 1 and Figure SI-2B), as required to provide a minimum handling ability (refer to SI-S1). While the grammage chosen for Nylon 66 mat is lower than the other nanofibrous mats (16.5–19.5 g/m^2, mean values) because it appears to be the limit for a complete mat impregnation with the prepreg resin.

3.1. Mode I and Mode II interlaminar fracture toughness evaluation of nano-modified CFRPs

Laminate CFRP fracture resistance was determined under Mode I and Mode II loading configurations, via Double Cantilever Beam (DCB) and End-Notched Flexure (ENF) tests, respectively. While in the DCB test the specimen is subjected to a perpendicular load respect to the crack propagation plane (Mode I, opening), in the ENF test a bending deformation is imposed to simulate the sliding of the two constituent specimen beams (Mode II, sliding). For a better understanding of the results, the crack propagation (and consequently the energy release rate, G, associated to) is split into two stages: the initiation stage (G_C), in which the delamination onset starts from the artificial crack, and the propagation stage (G_R). In propagation, the energy was evaluated considering a crack length (a) between 48 and 90 mm for Mode I, and the 32–42 mm range for Mode II tests. It is to underline that during DCB tests of CFRPs modified with rubber-containing layers, the designed crack plane (i.e. the central one) was not guaranteed to be the unique present, being possible the formation of an additional crack plane adjacent to this. If this occurred, the resulting $G_{I,R}$ was calculated by averaging only the points associated to the crack propagation in the modified interface to exclude any interference, reducing the abovementioned crack length range (Table SI-4). Mode I and Mode II results (maximum load and calculated energy release rate) are listed in detail in Table SI-5.

Fig. 3A shows the representative DCB load vs. displacement curves of the pristine sample (C-Ref) and of all the modified composite panels. The nano-modified laminates have a similar trend and slope of the corresponding reference until the first force drop occurs. However, the presence of the interleaved nanofibers, except for the PCL ones, clearly postpone the crack initiation and increase the maximum force. Indeed, the average maximum load (Fig. SI-4A) is significantly and statistically higher for the CFRPs interleaved with rubbery nanofibers: from +53% to +104% (C-20/80 and C-60/40, respectively), while a composition-related threshold at 40%wt of NBR appears, beyond which increasing the rubber fraction in the interleaved material does not correspond to a further performance enhancement.

In fact, the use of pure rubber film (C-*f*-NBR) is not dramatically helping further the performance with respect to the blended nanofibers (Fig. 3B), in spite of the grammage that for the film is almost double

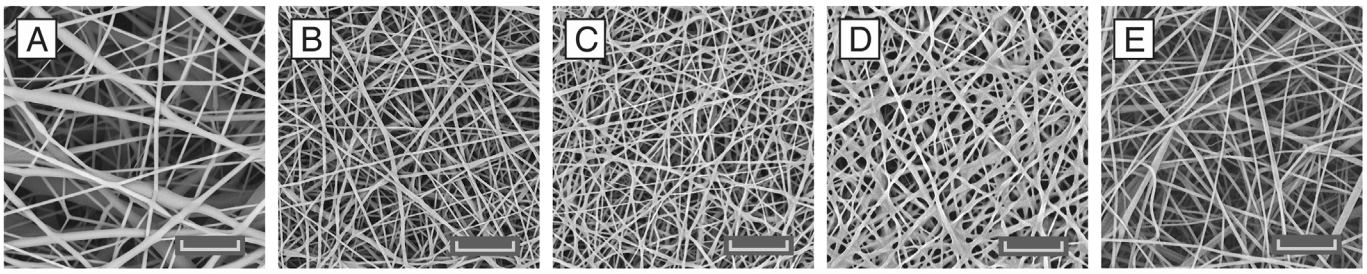

Fig. 2. – SEM micrographs of nanofibrous mats interleaved in CFRP laminates: A) *n*-PCL, B) *n*-20/80, C) *n*-40/60, D) *n*-60/40 and E) *n*-NYL. Scale bar: 6 μm, 5000×.

(Table 1 and Figure SI-2B). After the first force drop, the presence of rubbery nanofibrous mat leads to load-displacement curves with a highly jagged profile and higher load mean values, accounting for a more complex delamination propagation pattern, characterized by multiple and subsequent crack advancements (Fig. 3A). This behaviour is confirmed by the micrograph analysis of the crack path (see Fig. 4). In Fig. 3B the *R*-curves (fracture toughness vs. crack length curves) resulting from the Mode I test are shown for the same representative specimens previously discussed. Their trends strengthen the hypothesis of a major hinder to CFRP delamination provided by NBR/PCL rubber nanofibers. Once again, the graph highlights two different "groups" of behaviour, i.e. with or without the rubber component in the composite. All the calculated G_I points (considering the test repetitions too) for rubbery-reinforced CFRPs, regardless of the NBR fraction, are above 1100 J/m^2, a value well higher than the performances of C-Ref, both in initial and propagation stages ($G_{I,C} = 373 \pm 16$ J/m^2 and $G_{I,R} = 642 \pm 75$ J/m^2). The lower limit jumps to 1900 J/m^2 when discarding the C-20/80 sample, supporting the idea of a NBR threshold in the blend nanofibrous mat above which only a slight increase in the mean values of both $G_{I,C}$ and $G_{I,R}$ can be found, as already observed for the maximum force behaviour. Assuming unitary the performances of the reference CFRP, the presence of NBR in the nanofibers in the 40–60%wt range dramatically affects the $G_{I,R}$ regardless of the actual liquid rubber content (increase of 320–340%, Fig. 3C), while the $G_{I,C}$ is more sensitive to the NBR content in the whole

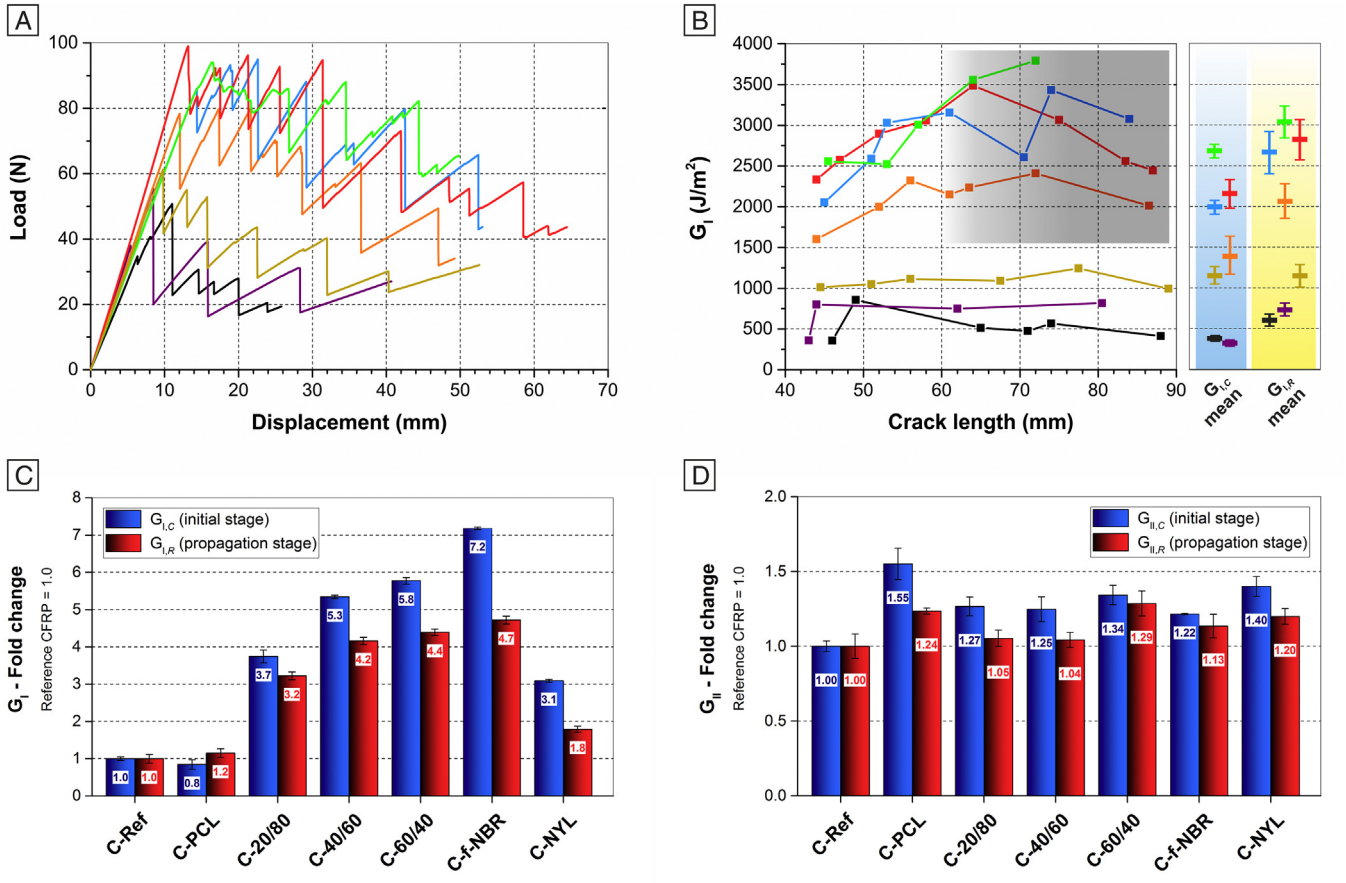

Fig. 3. – DCB tests results: A) load-displacement curves; B) *R*-curves related to the same specimens displayed in A), besides the $G_{I,C}$ and $G_{I,R}$ average values. The shadow approximately indicates the crack range excluded for $G_{I,R}$ calculation of rubber-containing samples. Colours: black C-Ref, purple C-PCL, orange C-20/80, light blue C-40/60, red C-60/40, light green C-*f*-NBR, yellow C-NYL. C) average G_I fold change (initial and propagation stages). D) ENF test results: average G_{II} fold change (initial and propagation stages). Bars in C) and D) are expressed as the relative variation of the value with respect to the reference sample (C-Ref), whose value is set as 1.0. (For interpretation of the references to colour in this figure legend, the reader is referred to the web version of this article.)

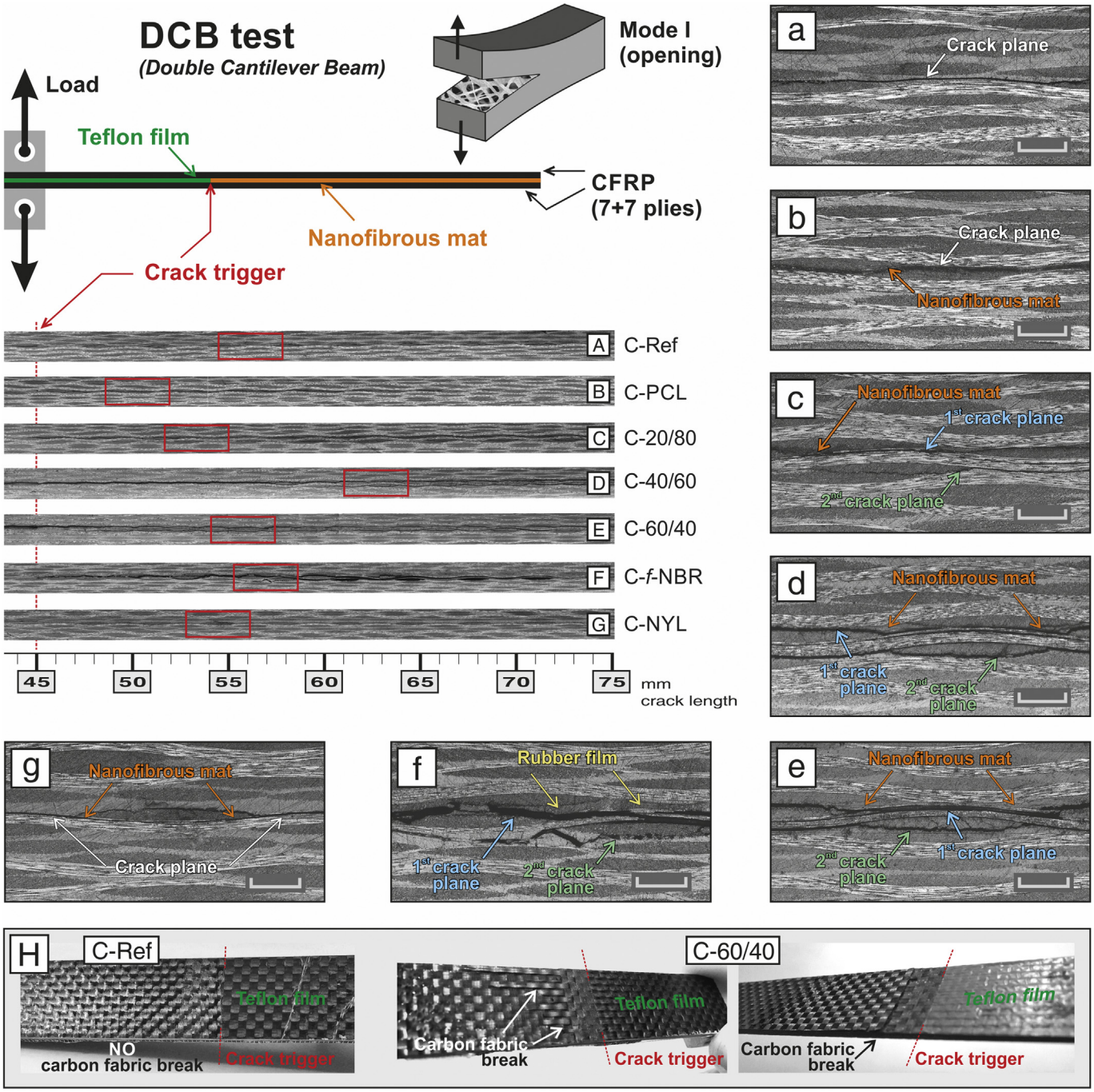

Fig. 4. – Micrographs of DCB specimens after the delamination tests. a)-g): enlargements (5×, scale bar 500 μm) of the red squared regions highlighted in the respective DCB specimen sections A)-G). H) Digital camera photographs of the delamination surfaces after DCB test of one representative rubber modified composite (C-60/40) and of the unmodified CFRP (C-Ref). (For interpretation of the references to colour in this figure legend, the reader is referred to the web version of this article.)

studied composition range, displaying an increasing trend for increased NBR fractions (from +270% for C-20/80 to +620% for the rubber film). However, the use of pure NBR film brings a very limited further positive effect on the Mode I propagation stage (+370%) respect to C-60/40 (+340%), but at the cost of severe membrane handling issues during the lamination process, the impossibility to produce low-grammage films as explained in SI-S1, as well as significant drop in the thermomechanical properties, as discussed later in Section 3.2. The use of PCL nanofibers (*n*-PCL), on the contrary, leads to Mode I delamination performance statistically comparable to the unmodified CFRP, thus suggesting that the presence of the rubbery component is the main responsible for such impressive boost in the delamination hampering ability. Such a toughening effect of the rubbery nanofibers is clearly displayed by the *R*-curves (Fig. 3B), where CFRPs with blend nanofibers show a higher number of subsequent crack propagation, denoting a more efficient ability to hinder delamination. The obtained results will be later compared with literature data gathered in a previous review [15].

The Mode I test results are confirmed by the micrograph analysis of the crack path (Fig. 4).

Micrographs show an almost "linear" crack propagation in the central interface for unmodified C-Ref, as well as for C-PCL, while the

CFRPs reinforced with rubbery nanofibers display a more complicated and an uneven crack path. This substantial change in the crack propagation behaviour is already present in the C-20/80 sample but becomes more evident starting from C-40/60 laminate. It is worth noting that the crack propagation occurs in the designed interlaminar plane (i.e. the central interface with the Teflon triggered crack), except for the rubbery modified samples where it extends also to the adjacent unreinforced interfaces. The crack, indeed, follows the path of least resistance and it is found to propagate across the very stiff woven carbon fabric, breaking it, instead of keep spreading along the initially designed fracture plane modified with the toughening layers (Fig. 4c-f).

In Fig. 5 SEM micrographs show the delamination surfaces of the previously discussed DCB specimens: while C-Ref displays the typical brittle fracture behaviour of epoxies characterized by wide flat planes (Fig. 5A3), the addition of PCL leads to some toughening of the matrix, showing a more corrugated matrix region (Fig. 5B3) and carbon fibers that tend to adhere more to the resin (Fig. 5B2). Such a modification, however, is not enough to hamper delamination, as DCB tests proved.

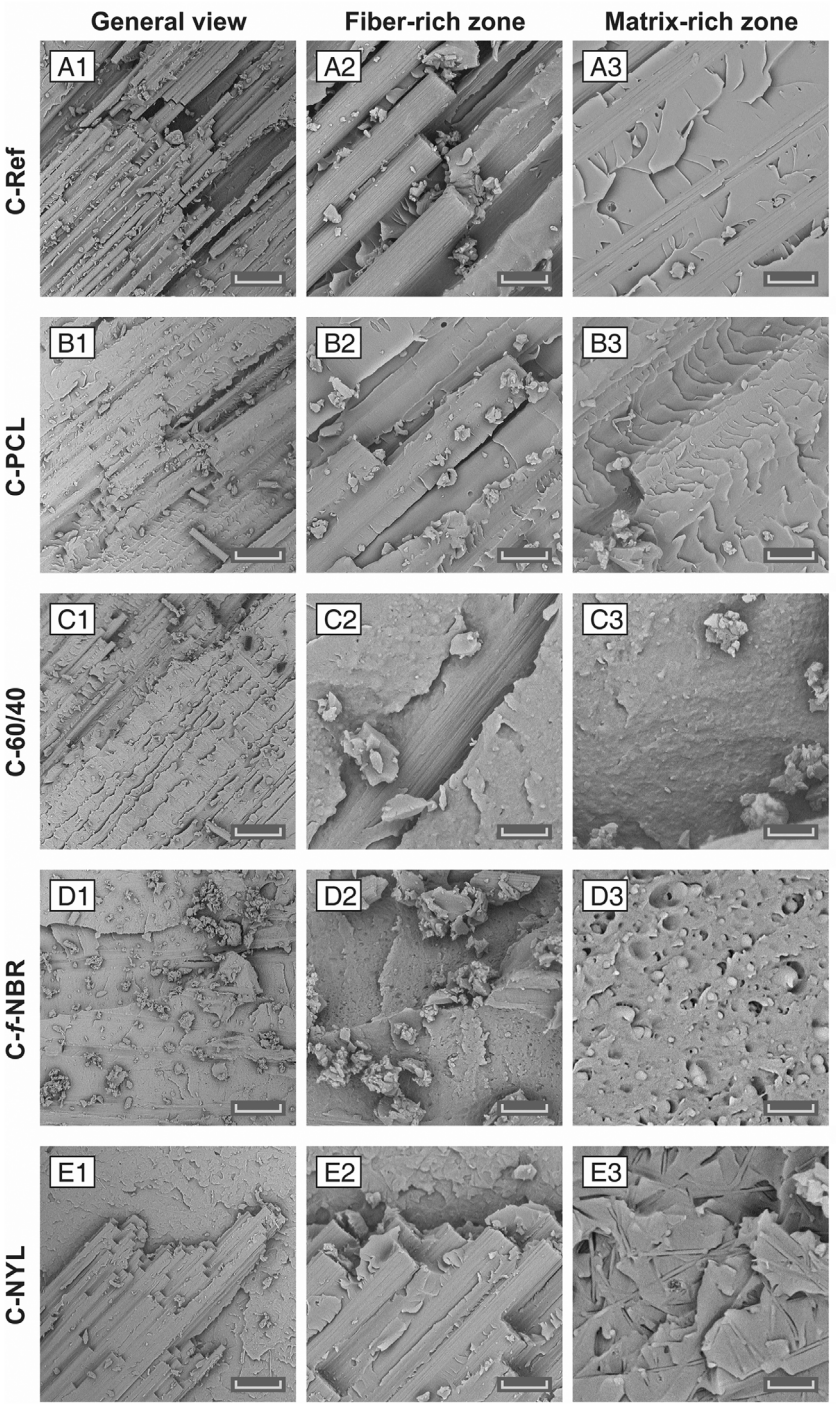

Fig. 5. – SEM micrographs of delamination plane of DCB specimens after the tests: general view of the fracture plane (column 1, 1000×, scale bar 50 μm), magnification of fiber-rich (column 2, 5000×, scale bar 10 μm except for image C2, 10000×, scale bar 5 μm) and matrix-rich (column 3, 5000×, scale bar 10 μm except for image C3, 10000×, scale bar 5 μm and for images D3-E3, 20000×, scale bar 2.5 μm) zones.

In Fig. 5C the delamination surface of the most representative composite with interleaved rubbery nanofibers, C-60/40, is reported: the very rough surface of the matrix (Fig. 5C3), reminiscent of strong plastic deformation, can be considered a sign of considerable crack branching. Moreover, carbon fibers stay well embedded in the matrix (Fig. 5C2), with no evidence of easy fiber pull out. An even rougher surface, that upon delamination presents also some spheres and holes morphology, is reported for the laminate with interleaved NBR film, where almost no naked carbon fibers can be detected (Fig. 5D). These observations confirm the rubber toughening action toward the epoxy resin, which reflects on increased energy release rate as calculated by DCB tests. In the CFRP modified with Nylon 66 mat (Fig. 5E), instead, no sign of matrix plasticisation is clearly detected, while nanofibers morphology is still evident, differently from all the previously discussed samples. This latter behaviour was however expected, based on the thermal properties of the different applied nanofibrous mats (the melting temperature of Nylon 66 is around 260 °C [28]). In this case, the fracture toughening enhancement should be attributed to the fiber bridging mechanism.

While the enhancement on the Mode I interlaminar fracture toughness is impressive (up to 5.8 times the reference value), the action of rubbery nanofibrous mats on the Mode II fracture energy is not as relevant (Fig. 3D and Fig. SI-5). All the modified samples display an improvement in $G_{II,C}$ in the 20–60% range, while the impact on $G_{II,R}$ is less remarkable. Overall the NBR/PCL nanofiber modified CFRPs display a similar performance at low NBR contents (C-20/80 and C-40/60), with a slight increase in the action against delamination at the initial stage; the performance however improves in C-60/40 that displays $G_{II,C}$ similar to C-NYL and a higher $G_{II,R}$ comparable to C-PCL (+34% and +29%, respectively, with respect to C-Ref). The latter, indeed, shows the best overall performances (+55% in $G_{II,C}$ and +24% in $G_{II,R}$).

These results well compare with the performance enhancements of many samples previously reported in the literature [15], as depicted in the graphs displayed in Fig. 6. The proposed nano-modification of the interlayer, with rubbery nanofibers, has a dramatic impact on the composite delamination under Mode I loading, and in particular at the initiation stage ($G_{I,C}$), while in Mode II loading the G_{II} values are just slightly higher than the reference material in most of the cases. The effect of the rubber on the Mode II delamination crack path, which again displays a jagged profile (Fig. SI-6), is similar to the observed one in DCB micrographs after testing. However, in this case, no failure of carbon fiber fabric occurred.

It is well known, and long since, that an increase of fracture toughness of the neat resin (in form of bulk without carbon fibers) has a lower effect on Mode II delamination fracture toughness than on Mode I when it is used on composite laminates [29]. This behaviour has been attributed to the different stress field distribution ahead of

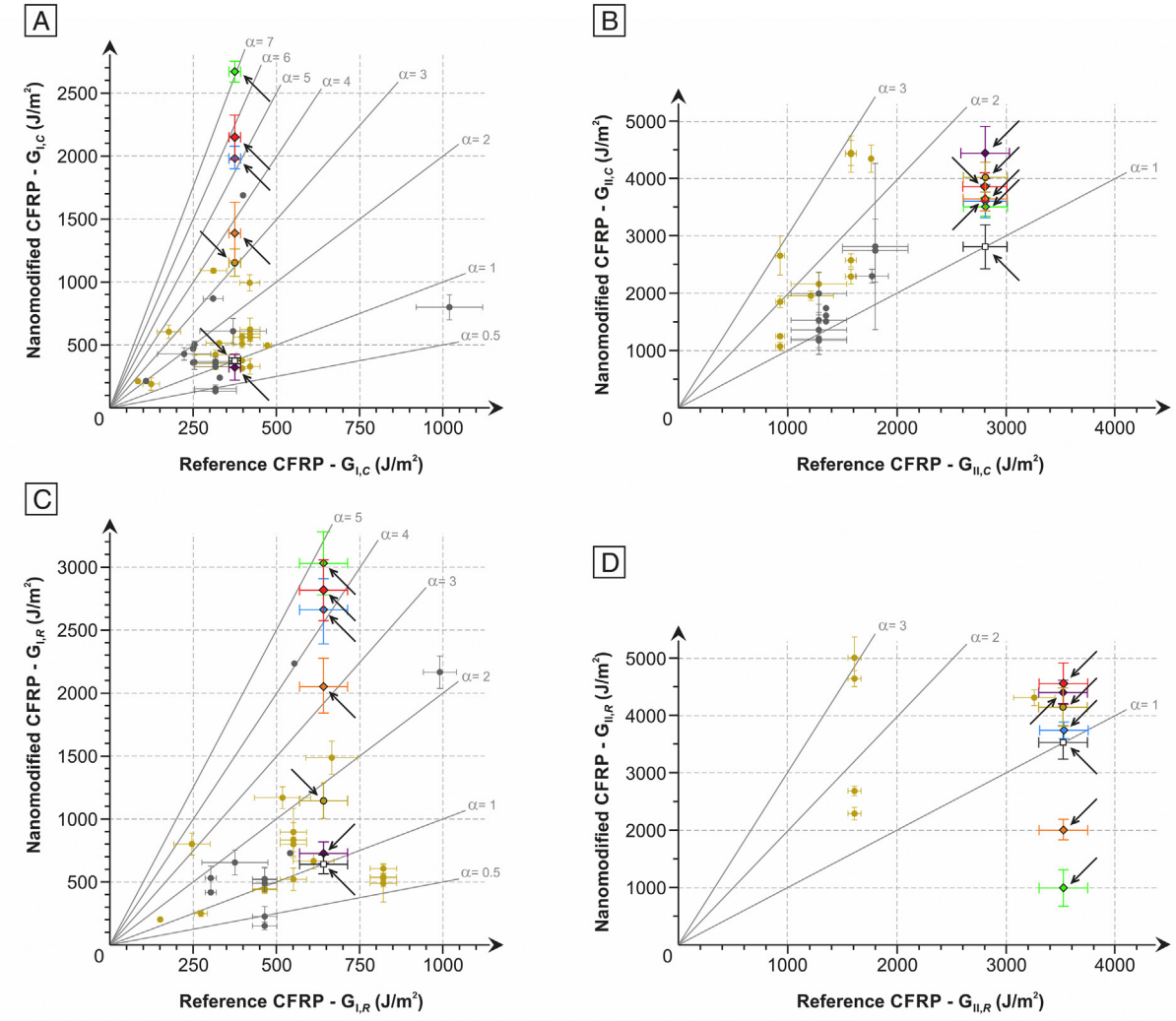

Fig. 6. – Mode I (A, C) and Mode II (B,D) energy release rate of the tested composites (marked by arrows) compared to literature data [15] (yellow for CFRP modified with polyamide nanofibers, gray for "other" nanofiber types). Tested CFRPs: white C-Ref, purple C-PCL, orange C-20/80, light blue C-40/60, red C-60/40, light green C-*f*-NBR, yellow C-NYL. α represents the ratio between G nanomodified and G reference. (For interpretation of the references to colour in this figure legend, the reader is referred to the web version of this article.)

the crack tip for Mode I and II. In Mode I the stress at the crack tip is highly concentrated with a high gradient, therefore the presence of a tougher resin can help, by plasticizing, to blunt the crack tip and redistribute the stress. Differently, in Mode II the stress is naturally redistributed ahead of the crack tip, thanks also to the laminar morphology of the composite, thus resulting in a less effect of a tougher resin on interlaminar fracture toughness. This behaviour was found in the laminates toughened with the present rubbery nanofibers too. It was also reported that the loss of fibrous morphology of the interleaved material, which is the case of "liquid" rubbery nanofibers, may detrimentally affect the composite performance in Mode II, while Mode I fracture toughness is not particularly sensitive to this phenomenon [30,31].

It can be concluded that by increasing the percentage of rubber in NBR/PCL blended nanofibers, the Mode I interlaminar fracture toughness increases ($G_{I,C}$ ranges between +270% and +480%, $G_{I,R}$ between +220% and +340%), while a slight variation (about +30%) of Mode II fracture toughness was observed for C-60/40.

3.2. Thermomechanical properties and damping evaluation of nano-modified CFRPs via dynamic mechanical analysis (DMA)

The ability to viscoelastically deform might contribute to introduce some damping ability into the otherwise extremely stiff CFRP with the aim of hamper and delay crack triggering and, in turn, delamination. Several test methods are available to determine the damping of a material. DMA is a simple and fast way to assess the dynamic behaviour of materials: tanδ value, i.e. the ratio between E" and E' (loss and storage moduli, respectively), is often addressed as "damping factor", and indeed accounts for the ability of the material to dissipate energy. Besides, DMA allows to determine the composite glass transition temperature (T_g), and the effective temperature region span of tanδ peak, all parameters useful to characterize the damping behaviour. Plain cross-linked NBR shows high damping at room temperature, thanks to its viscoelastic nature [23], PCL has some damping properties too, because they both are well above their glass transition, and thus able to dissipate energy via molecular rearrangements. By mixing NBR and PCL in different proportions, it may be possible to modulate the loss factor of the resulting blend, depending also on the extent of crystal phase present in it. In this case, however, a DMA evaluation of the performance of the pristine nanofibrous mat would be ineffective in terms of damping efficiency assessment, since in the composite the nanofibrous morphology is lost, as demonstrated by SEM micrograph (Fig. 5B-C), and the polymers are found dispersed in the epoxy matrix, thus losing the dissipation mechanism associated to the fibrous arrangement [28]. Hence nanofibrous mats were directly integrated in CFRPs to evaluate their effect on dynamic-mechanical properties via DMA. Two very different configurations were tested, characterized by 10 CFRP plies with membranes interleaved only in the central interface and in all the interfaces, using the IMP503Z resin system, together with some laminate configurations with the IMP503Z-HT resin system (Table 2).

Besides the evaluation of the thermomechanical properties of the composite, the DMA is also useful to investigate nanofibers impact on the resin behaviour, contributing to better understand the blend/resin mixing process.

Unmodified CFRP (C-Ref) displays a single significant relaxation process, which can be safely attributed to the glass transition. Such a relaxation, clearly detected as a peak in the tanδ curve around 129 °C (T_α), is narrow and symmetrical, suggesting a good curing of the resin.

The lamination sequence with a single interleaved membrane provides a main significant relaxation T_α positioned at a comparable temperature (125–129 °C), and a conservative modulus (E') that is practically unaffected below T_g (Table 2 and Fig. 7A). However, just one modified interface with PCL or rubbery nanofibers impacts on the onset of the E' drop, which represents another way to determine the glass transition of a material: this is a more conservative approach for evaluating glass transition than tanδ peak, being the E' onset the temperature extrapolation at which the storage modulus drop begins. The curves show the E' onset lowering becomes more important for increasing NBR fraction in the nanofibers (82 °C for C-60/40 instead of 116 °C of C-Ref), and 53 °C for the laminate with NBR film (C-*f*-NBR). Details are reported in Table 2.

Hence, to investigate the maximum membranes impact (at the considered grammage) on the CFRP thermomechanical properties, each ply interface but the external ones was modified with nanofibers, besides with NBR film (Fig. SI-1B). The overall weight variation is in the 2–3% wt range, and roughly represents 5–10%wt with respect to the resin fraction. C-NYL displays a behaviour practically identical to C-Ref (Fig. 7B): indeed, highly crystalline glassy nanofibrous mat does not affect the resin viscoelastic relaxation, and the limited weight fraction (about 2%wt) does not made the highly crystalline Nylon 66 glass transition detectable in the DMA spectrum.

Such a behaviour well compares with the observations drawn upon analysing fracture surfaces of the DCB tested samples, where no signs of resin plasticization were evidenced. C-PCL shows, instead, a different behaviour. Although the storage modulus (E') seems to display a single relaxation, the width of such transition is wider and begins at a decisively lower temperature than C-Ref and C-NYL. Moreover, the tanδ shows a complex multipeaked profile with a high-T shoulder matching

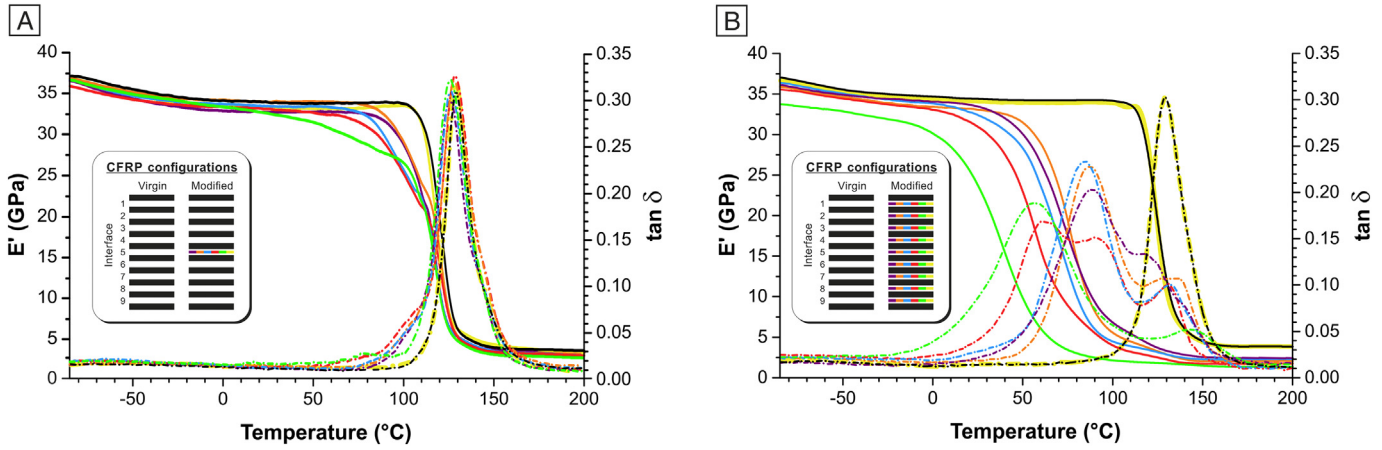

Fig. 7. – E' (solid lines) and tanδ (dashed lines) representative curves of CFRP samples characterized by A) only the central interface modified and B) all the 9 interfaces modified. Colours: black C-Ref, purple C-PCL, orange C-20/80, light blue C-40/60, red C-60/40, light green C-*f*-NBR, yellow C-NYL. Inset box: tested CFRP configurations (thick lines: CFRP plies, thin lines: interleaved membranes, with colours as stated before). (For interpretation of the references to colour in this figure legend, the reader is referred to the web version of this article.)

the epoxy resin T_α and a lower-T peak at 89 °C that, by both the intensity and the position, cannot be ascribed to the sole PCL fraction crystal melting (2–3%wt overall PCL content, melting temperature 60 °C [24]). The C-*f*-NBR composite displays a somehow similar profile with respect to C-PCL, showing once again a less intense high-T peak corresponding to the epoxy T_α and an even lower-T (58 °C) main relaxation phenomenon. Both composites display a main intense relaxation in a position that does not belong to their respective glass transitions (which are in both cases well below 0 °C [24]), neither to the PCL crystal phase melting, as previously observed in phase separated epoxy/PCL samples [32]. While, indeed, a wealth of papers [8,32,33] reports reaction-induced phase separation in both epoxy/PCL and epoxy/NBR systems, this does not appear to be the case. Instead, a phase separated system would display in DMA spectra an intense α relaxation due to the resin glass transition and some less intense phenomena due to the main thermal transition of the minor component(s), being it PCL or NBR. On the other side, when a component of plasticizing ability is mixed with a polymer it is renown that a broadening of its α-peak occurs. The lack of such different characters in the tanδ spectra in favor of an intermediate behaviour in between the two extreme components (with a prevalence of the epoxy resin, as expected) accounts thus for some miscibility in both systems. This view is supported by some recent literature [30,34] that reports core-shell nanofibers with the outer shell based on PCL to allow for thermoplastic melting and diffusion within the epoxy, leading to some positive toughening action. Composites modified with NBR/PCL nanofibrous mats show a behaviour similar to the one of C-PCL for compositions up to 40%wt NBR, while further increase of the rubbery fraction (60%wt) leads to the appearance of an additional relaxation positioned at a temperature comparable with C-*f*-NBR low-T phenomenon. Assuming that the polymers from nanofibers melt (PCL) and diffuse (PCL and NBR) into the epoxy matrix during curing cycle, the latter formulation (C-60/40) seems to display two different phases reminiscent of the previously discussed epoxy/PCL and epoxy/NBR blends. The presence of the highly damping NBR component further widens the energy dissipation window of the composites down to below room temperature and might also promote some phase separation with a mixed composition, that would explain the appearance, in the fracture surface, of the observed globular morphology. The latter hypotheses are strengthened by the aspect of the delamination surfaces previously discussed (Fig. 5) after the attempt at washing them with chloroform, in order to remove soluble polymeric fractions. Literature indeed reports extremely peculiar spherical of interpenetrated morphologies of the phase separated component, that can be easily highlighted upon selective removal of one component. Such peculiar

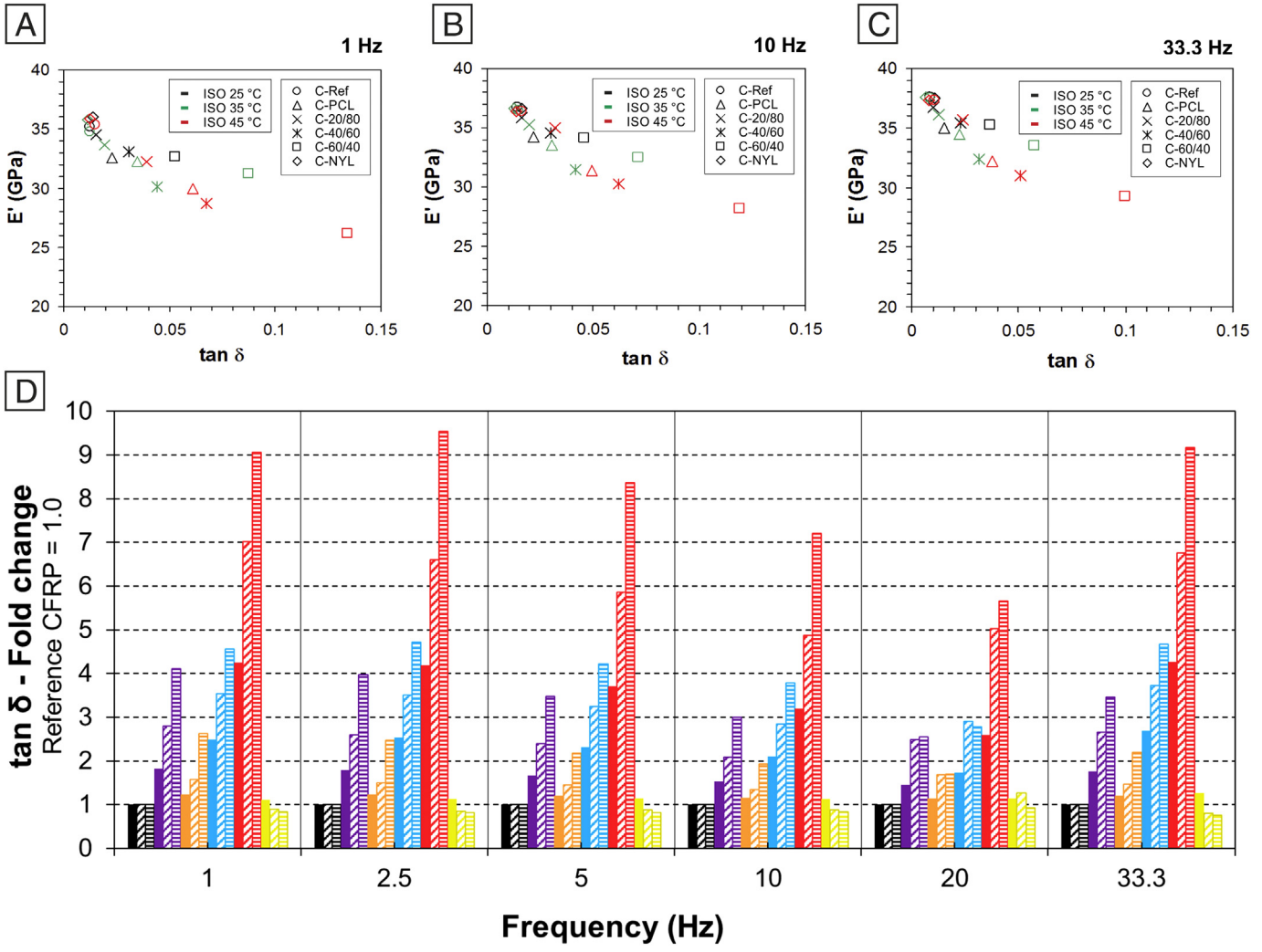

Fig. 8. – E' vs tanδ graphs for CFRPs tested under isothermal conditions at 1 Hz (A), 10 Hz (B) and 33.3 Hz (C). D) Relative variation of tanδ for different CFRPs at various frequencies and isothermal temperatures (solid bar 25 °C; oblique dashed bar 35 °C; horizontal dashed bar 45 °C). Colours: black C-Ref, purple C-PCL, orange C-20/80, light blue C-40/60, red C-60/40, yellow C-NYL. 50 Hz data are not displayed because of no positive tanδ values detected for C-Ref at this frequency. (For interpretation of the references to colour in this figure legend, the reader is referred to the web version of this article.)

morphologies do not appear in the present samples (Fig. SI-7), with the exception of the one modified with NBR film, where the small spheres seem to be removed, leaving some holes.

Damping capacity of the same CFRP samples was thus investigated in isothermal conditions (25, 35 and 45 °C), under a wide range of testing frequencies (1 - 2.5 - 5 - 10 - 20 - 33.3 - 50 Hz). Results are summarized in Fig. 8, showing the trend of relative variation of nanomodified CFRPs with respect to C-Ref sample (in Table SI-6 tanδ values of tested samples for various conditions are reported, while in SI-S4 absolute values in isothermal conditions are also displayed and commented).

The data clearly show that temperature strongly affects the damping factor. The higher the temperature, the higher the tanδ value is for a considered frequency and CFRP type. In particular, the effect is higher for composites with high NBR fractions in mats. Also testing frequency influences tanδ value (Fig. SI-8). Fig. 8A-C reports stiffness-loss maps [35] evaluated at different frequencies and temperatures. This way of representing mechanical performances of the CFRPs highlights the effect that different additive systems have on mechanical behaviour and how, with the present approach, it is possible to tune and tailor the performance of the final laminates.

The main drawback of the widespread use of such rubbery nanofibers in CFRPs resides in the lowering of E' onset (Table 2), which may strongly limit the use of toughened laminates. Of course, all the applications which involve low service temperature are not affected by this problem. On the contrary, composites may benefit from reduced matrix brittleness, which makes more difficult the microcracks formation and propagation [22]. However, one of the advantages of using nanofibrous membranes to toughen the composites is the fact that they can be conveniently positioned, during lamination, in the critical regions, without modifying the whole mass of the object. They can be applied for tailored and localized modification only in critical areas where interlaminar stresses are mostly concentrated due to geometric discontinuities, such as free edges, holes, ply-drops and adhesive bonding [18]. Contrarily to the use of bulk toughened matrix, the mat interleaving approach allows to preserve the average thermomechanical properties of the whole component.

Moreover, both the grammage and the matrix characteristics may be accurately chosen to tailor the laminate properties in terms of storage modulus, T_g, damping and delamination performance, depending on the application requirements.

With the aim of better understanding the impact of such rubbery nanofibers on the CFRP thermomechanical properties, some additional CFRP panels were produced using a different resin (a "High Temperature" HT epoxy, IMP503Z-HT resin system) for evaluating the effect on a hosting material with different properties. In this case, the most promising mat candidate (*n*-60/40) for what concerns the CFRP fracture toughness and damping improvement, but also the most problematic one because of the lowering of CFRP T_g, was selected. The *n*-60/40 mat was used to modify, again, all the interfaces and just the central one (Fig. 9, green curves, and Fig. 9B, gray curves, respectively) of a 10 plies CFRP panel. Moreover, an additional panel was produced with 5 nanofibrous membranes positioned at the 1-3-5-7-9 interlayers (Fig. 9B, magenta curves).

A direct comparison of the effect of *n*-60/40 mat on the two applied epoxy resin systems demonstrates a very similar effect: Fig. 9A displays the behaviour of the two reference unmodified composites (C-Ref and C-Ref-HT) with the relative 9-membrane-interleved ones (C-60/40 and C-60/40-HT_9).

While the HT resin has a slightly higher glass transition temperature (T_α = 150 °C, E' onset at 122 °C), the effect of the NBR-rich nanofibers (C-60/40-HT_9) is highly reminiscent of the C-60/40 sample: in both cases a high-T relaxation typical of the unmodified epoxy is still present together with two low-T peaks that, according to the previous interpretation might be due to the PCL-rich and NBR-rich regions. This behaviour is also observed to a minor extent in composites with a lower amount of modification. In particular, the placement of 5 interleaved membranes leads to a lesser widening of the tanδ peak toward low-T (C-60/40-HT_5). This trend holds in the single membrane modified CFRP (C-60/40-HT_1). It is worth noting that even if the E' onset moves toward lower temperature when increasing the number of nano-modified interfaces, the reached T_g temperature (E' onset) depends also on the properties of the hosting matrix. While the addition of only one *n*-60/40 mat in the resin system IMP503Z determines a shift of the E' onset from 116 °C to 82 °C, in presence of the HT resin version the same mat causes a drop at 103 °C, starting from 122 °C of the unmodified laminate (C-Ref-HT). A similar trend is observed when all the interfaces are nano-modified: E' onset at 40 °C for the IMP503Z resin and 61 °C for the HT resin. The CFRP with 5 mats interleaved displays an intermediate behaviour with respect to the two extreme CFRP configurations (E' onset of 72 °C). These observations point at demonstrating an important role of the hosting resin system too on the resulting laminate thermomechanical properties, in addition to all the other presented variables, i.e. NBR percentage in the nanofiber and number of modified interfaces, but also the extreme versatility of the rubbery nanofibrous membranes that are able to significantly modify different matrices.

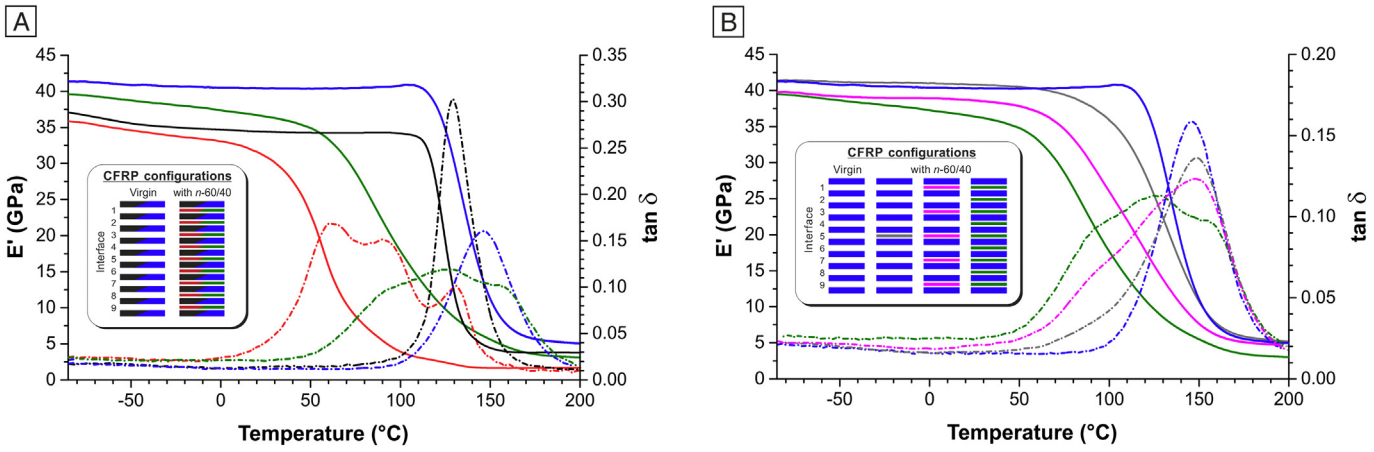

Fig. 9. – A) DMA of unmodified CFRP (C-Ref with IMP503Z resin system and a reference with the "High Temperature" HT resin, black and blue curves, respectively) and CFRP with 9 membranes *n*-60/40 interleaved (red curves IMP503Z resin, green curves with IMP503Z-HT resin. B) Comparison of different configurations of CFRPs with the "HT" resin system: unmodified CFRP (blue), and with interface 5 (gray), interfaces 1-3-5-7-9 (magenta) and all interfaces (green) modified. (For interpretation of the references to colour in this figure legend, the reader is referred to the web version of this article.)

4. Conclusion

The interleave of NBR/PCL blend nanofibrous mats during CFRP lamination proved to be a powerful tool to hinder delamination of epoxy-based CFRP laminates via localized resin toughening without significantly affecting weight and dimension of the laminate. A dramatic increase of the energy release rate (G) at the initiation and propagation stages (up to 5.8× and 4.4× the reference values, respectively) is observed. Acting on the hinder of crack initiation represents a major safety parameter since, once a crack starts, the laminate is already compromised and unrepairable. Nonetheless, reducing crack propagation helps to increase the safety and lifetime of the component. Rubbery nanofibers demonstrated the ability to significantly impact Mode I delamination (up to +480% of G_I), while in Mode II the improvement is limited (up to +34% of G_{II}). The rubbery mats are also able to blend with the epoxy matrix during curing, providing a significant modification of the damping ability. By increasing the NBR content, the composite damping increases, but at the expenses of a decreased maximum operating temperature (lowering of E' onset, T_g). The system proved to be easily tailorable, depending on the specific application, simply acting on the percentage of rubber in the fiber in order to best compromise between damping and maximum operating temperature.

Such promising results pave the way to the application of rubbery nanofibrous mats for localized modification of laminates in critical spots, such as free edges, holes, ply-drops and adhesive bonding, providing a flexible and easy system to be integrated in the composite during the lamination process.

Another important parameter, which could affect the tanδ, E' onset (T_g) and fracture toughness, is the grammage of the interleaved mat, which should be explored in the future for a thoroughly evaluation of the rubbery nanofibers effect on thermomechanical properties of laminates.

Declaration of Competing Interest

None.

Acknowledgment

Authors wish to acknowledge the project “TEAM SAVE – E91B18000460007” (PG/2018/632196) in the framework of POR FESR 2014-2020 funded by Regione Emilia-Romagna with DGR 986/2018 for financial support.

The raw/processed data required to reproduce these findings cannot be shared at this time as the data also forms part of an ongoing study.

Appendix A. Supplementary data

Supplementary data to this article can be found online at https://doi.org/10.1016/j.matdes.2020.109049.

References

[1] D. Geng, Y. Liu, Z. Shao, Z. Lu, J. Cai, X. Li, X. Jiang, D. Zhang, Delamination formation, evaluation and suppression during drilling of composite laminates: a review, Compos. Struct. 216 (2019) 168–186, https://doi.org/10.1016/j.compstruct.2019.02.099.

[2] N. Takeda, S. Ogihara, S. Suzuki, A. Kobayashi, Evaluation of microscopic deformation in CFRP laminates with delamination by micro-grid methods, J. Compos. Mater. 32 (1998) 83–100, https://doi.org/10.1177/002199839803200105.

[3] S.U. Khan, C.Y. Li, N.A. Siddiqui, J.K. Kim, Vibration damping characteristics of carbon fiber-reinforced composites containing multi-walled carbon nanotubes, Compos. Sci. Technol. 71 (2011) 1486–1494, https://doi.org/10.1016/j.compscitech.2011.03.022.

[4] M.D. Rao, Recent applications of viscoelastic damping for noise control in automobiles and commercial airplanes, J. Sound Vib. 262 (2003) 457–474, https://doi.org/10.1016/S0022-460X(03)00106-8.

[5] R. Bagheri, B.T. Marouf, R.A. Pearson, Rubber-toughened epoxies: a critical review, Polym. Rev. 49 (2009) 201–225, https://doi.org/10.1080/15583720903048227.

[6] E.B. Caldona, A.C.C. De Leon, B.B. Pajarito, R.C. Advincula, A review on rubber-enhanced polymeric materials, Polym. Rev. 57 (2017) 311–338, https://doi.org/10.1080/15583724.2016.1247102.

[7] C.K. Riew, A.R. Siebert, R.W. Smith, M. Fernando, A.J. Kinloch, Toughened Epoxy Resins: Preformed Particles as Tougheners for Adhesives and Matrices, in: Toughened Plast. II, American Chemical Society, 1996: pp. 33–44.

[8] R.J.J. Williams, B.A. Rozenberg, J. Pascault, Reaction-induced phase separation in modified thermosetting polymers (1997)https://doi.org/10.1007/3-540-61218-1_7.

[9] C.W. Wise, W.D. Cook, A.A. Goodwin, CTBN rubber phase precipitation in model epoxy resins, Polymer (Guildf). 41 (2000) 4625–4633, https://doi.org/10.1016/S0032-3861(99)00686-2.

[10] Y.A. Dzenis, D.H. Reneker, Delamination resistant composites prepared by small diamerter fiber reinforcement at ply interface, US 6 (2001) 265,333.

[11] S. van der Heijden, L. Daelemans, B. De Schoenmaker, I. De Baere, H. Rahier, W. Van Paepegem, K. De Clerck, Interlaminar toughening of resin transfer moulded glass fibre epoxy laminates by polycaprolactone electrospun nanofibres, Compos. Sci. Technol. 104 (2014) 66–73, https://doi.org/10.1016/j.compscitech.2014.09.005.

[12] P. Akangah, S. Lingaiah, K. Shivakumar, Effect of Nylon-66 nano-fiber interleaving on impact damage resistance of epoxy/carbon fiber composite laminates, Compos. Struct. 92 (2010) 1432–1439, https://doi.org/10.1016/j.compstruct.2009.11.009.

[13] J. Zhang, T. Yang, T. Lin, C.H. Wang, Phase morphology of nanofibre interlayers: critical factor for toughening carbon/epoxy composites, Compos. Sci. Technol. 72 (2012) 256–262, https://doi.org/10.1016/j.compscitech.2011.11.010.

[14] D. Quan, F. Bologna, G. Scarselli, A. Ivankovic, N. Murphy, Mode-II fracture behaviour of aerospace-grade carbon fibre/epoxy composites interleaved with thermoplastic veils, Compos. Sci. Technol. 191 (2020).

[15] R. Palazzetti, A. Zucchelli, Electrospun nanofibers as reinforcement for composite laminates materials – a review, Compos. Struct. 182 (2017) 711–727, https://doi.org/10.1016/j.compstruct.2017.09.021.

[16] L. Sisti, J. Belcari, L. Mazzocchetti, G. Totaro, M. Vannini, L. Giorgini, A. Zucchelli, A. Celli, Multicomponent reinforcing system for poly(butylene succinate): composites containing poly(l-lactide) electrospun mats loaded with graphene, Polym. Test. 50 (2016) 283–291, https://doi.org/10.1016/j.polymertesting.2016.01.022.

[17] L. Mazzocchetti, T. Benelli, E. Maccaferri, S. Merighi, J. Belcari, A. Zucchelli, L. Giorgini, Poly-m-aramid electrospun nanofibrous mats as high-performance flame retardants for carbon fiber reinforced composites, Compos. Part B Eng. 145 (2018) 252–260, https://doi.org/10.1016/j.compositesb.2018.03.036.

[18] T.K. O'Brien, Delamination of composite materials, Compos. Mater. Ser. 4 (1991) 181–198, https://doi.org/10.1016/B978-0-444-70507-5.50009-3.

[19] F. Xu, X.S. Du, H.Y. Liu, W.G. Guo, Y.W. Mai, Temperature effect on nano-rubber toughening in epoxy and epoxy/carbon fiber laminated composites, Compos. Part B Eng. 95 (2016) 423–432, https://doi.org/10.1016/j.compositesb.2016.04.019.

[20] A.T. Nettles, E.J. Biss, Low temperature mechanical testing of carbon-fiber/epoxy-resin composite materials, NASA Tech. Pap. 3663. (1996).

[21] H. Kishi, M. Kuwata, S. Matsuda, T. Asami, A. Murakami, Damping properties of thermoplastic-elastomer interleaved carbon fiber-reinforced epoxy composites, Compos. Sci. Technol. 64 (2004) 2517–2523, https://doi.org/10.1016/j.compscitech.2004.05.006.

[22] T. Takeda, W. Fan, Q.P. Feng, S.Y. Fu, F. Narita, Y. Shindo, Cryogenic mechanical properties of woven glass/epoxy composites modified with multi-walled carbon nanotube and n-butyl glycidyl ether under tensile static and cyclic loadings, Cryogenics (Guildf). 58 (2013) 33–37, https://doi.org/10.1016/j.cryogenics.2013.09.005.

[23] Z.D. Xu, Y.X. Liao, T. Ge, C. Xu, Experimental and theoretical study of viscoelastic dampers with different matrix rubbers, J. Eng. Mech. 142 (2016) 1–12, https://doi.org/10.1061/(ASCE)EM.1943-7889.0001101.

[24] E. Maccaferri, L. Mazzocchetti, T. Benelli, T.M. Brugo, A. Zucchelli, L. Giorgini, Rubbery nanofibers by co-electrospinning of almost immiscible NBR and PCL blends, Mater. Des. 186 (2020). doi:https://doi.org/10.1016/j.matdes.2019.108210.

[25] R. Palazzetti, A. Zucchelli, I. Trendafilova, The self-reinforcing effect of nylon 6,6 nano-fibres on CFRP laminates subjected to low velocity impact, Compos. Struct. 106 (2013) 661–671, https://doi.org/10.1016/j.compstruct.2013.07.021.

[26] D5528–01 2001. Standard Test Method for Mode I Interlaminar Fracture Toughness of Unidirectional Fiber-Reinforced Polymer Matrix Composites, Am. Soc. Test. Mater. (2014) 1–13. doi:https://doi.org/10.1520/D5528-13.2.

[27] BS EN 6033:2015, BS EN 6034 : 2015 BSI Standards Publication Aerospace series — Carbon fibre reinforced plastics — Test method — Determination of interlaminar fracture toughness energy — Mode II — GIIC, BSI Stand. Publ. (2015) 14.

[28] E. Maccaferri, L. Mazzocchetti, T. Benelli, A. Zucchelli, L. Giorgini, Morphology, thermal, mechanical properties and ageing of nylon 6,6/graphene nanofibers as Nano^2 materials, Compos. Part B Eng. 166 (2019) 120–129, https://doi.org/10.1016/j.compositesb.2018.11.096.

[29] Application of Fracture Mechanics to Composite Materials, Elsevier, 1989. doi: https://doi.org/10.1016/B978-0-444-89079-5.50001-5.

[30] L. Daelemans, N. Kizildag, W. Van Paepegem, D.R. D'hooge, K. De Clerck, Interdiffusing core-shell nanofiber interleaved composites for excellent mode I and mode II delamination resistance, Compos. Sci. Technol. 175 (2019) 143–150, https://doi.org/10.1016/j.compscitech.2019.03.019.

[31] G.W. Beckermann, K.L. Pickering, Mode I and mode II interlaminar fracture toughness of composite laminates interleaved with electrospun nanofibre veils, Compos. Part A Appl. Sci. Manuf. 72 (2015) 11–21, https://doi.org/10.1016/j.compositesa.2015.01.028.

[32] A. Cohades, E. Manfredi, C.J.G. Plummer, V. Michaud, Thermal mending in immiscible poly(ϵ-caprolactone)/epoxy blends, Eur. Polym. J. 81 (2016) 114–128, https://doi.org/10.1016/j.eurpolymj.2016.05.026.

[33] G. Vanden Poel, S. Goossens, B. Goderis, G. Groeninckx, Reaction induced phase separation in semicrystalline thermoplastic/epoxy resin blends, Polymer (Guildf). 46 (2005) 10758–10771, https://doi.org/10.1016/j.polymer.2005.09.013.
[34] L. Daelemans, W. Van Paepegem, D.R. D'hooge, K. De Clerck, Excellent Nanofiber adhesion for hybrid polymer materials with high toughness based on matrix Interdiffusion during chemical conversion, Adv. Funct. Mater. 29 (2019) 1–10, https://doi.org/10.1002/adfm.201807434.
[35] M. Brodt, R.S. Lakes, Composite materials which exhibit high stiffness and high viscoelastic damping, adapted from 1995 1–11.